Appendices

Appendix A Acoustic Velocity Measurement Calibration

A two-microphone technique was used to measure the velocity perturbation of the flat flame burner. Khanna has elaborated in details about the two-microphone technique in theory in conjunction with the instrumental set up. [Kha01] Hereby, we only list the calibration procedure. Considering the gain of the integration circuitry and sensitivity of both microphones, a conversion constant from measured voltage value (volts) to the actual velocity unit (m/s) is calibrated. It is used to determine the actual input velocity amplitudes of the measured describing functions for our experiments.

The sensitivity of the two microphones is calibrated at 260.018 Pa/Volt. So the velocity perturbation u' can be computed as,

$$u' = \frac{260.018}{\rho \Delta x} \frac{u_v}{A(\omega)} \text{ (m/s)} \qquad \text{(A.1)}$$

where u_v is the velocity measured in volts, $\rho = 1.16$, $\Delta x = 0.055m$, and $A(\omega)$ is the gain of the circuit over a pure integrator ($1/\omega$) at frequency ω.

To determine $A(\omega)$, one input of the circuit was connect to ground and the other was input with 2mv random noise with bandwidth 0-1600Hz. Figure A.1 shows the frequency response of the integration circuit. For frequency f >12 Hz, the magnitude response rolled off –20dB/dec and phase response is about -90^o, which can be used as an integrator approximately. At frequency 180Hz, the gain of amplification circuit was computed as,

$$A(\omega) = \frac{13.3909}{1/(2\pi \times 180)} = 1.5145e4$$

Therefore, the conversion from voltage values to the actual velocity unit is,

$$k = \frac{260.018}{1.16 \times 0.055} \frac{1}{1.5145e4} = 0.2691 \text{ m/(s-V)}$$

With the velocity probe sensed 1 volts, it is equivalent to 0.269 m/s.

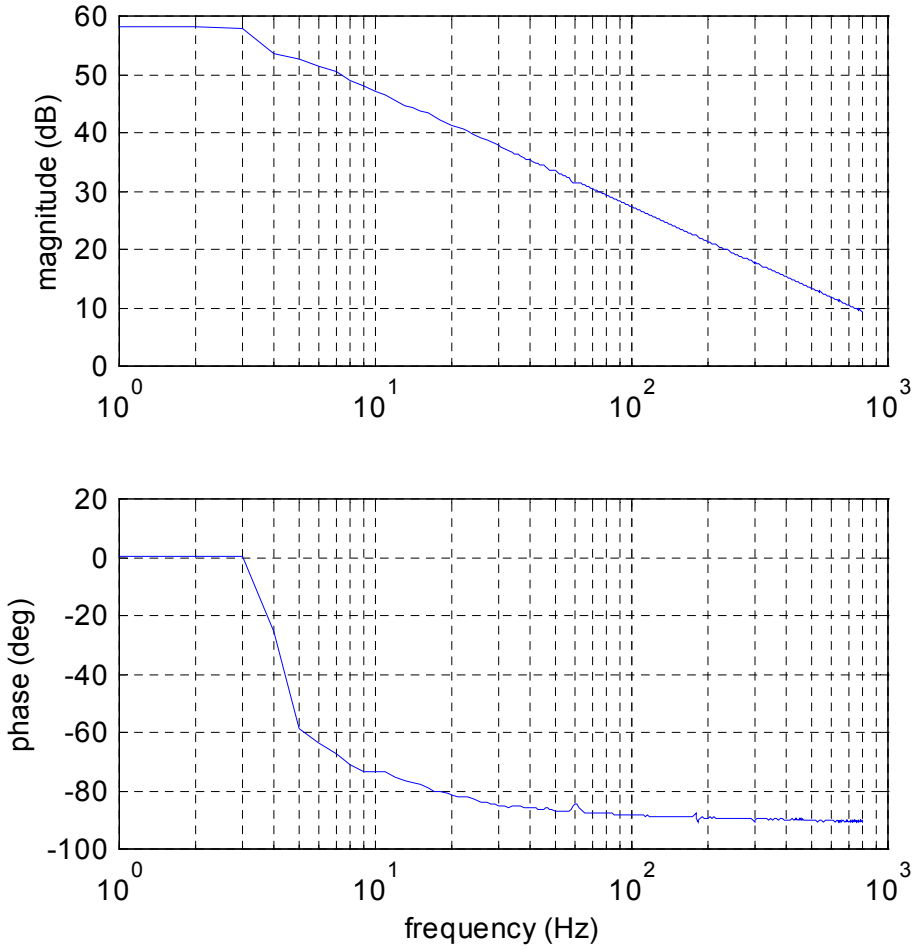

Figure A.1. FRF of velocity probe integration circuit to 2 mV random noise input

Appendix B. Rijke Tube Pressure Transducer Calibration

The pressure amplitudes for limit cycles of the Rijke tube were measured using pressure transducers. Due to the harsh environment, a high-sensitivity was not used to measure pressures when the combustor was running. Below we elaborate the procedures to calibrate the pressure transducers and obtain a constant to convert the sensed voltage value to actual pressure values in Pa or SPL.

The calibrator includes a high sensitivity microphone and a standard sound generator. It generated 1 Pa (~ 94dB SPL re 2e-5) and 10 Pa (~114dB SPL re 2e-5) sound, which can be used to verify the microphone sensitivity. With source amplitude of 1 Pa, the microphone measured –57.6 dBV. With a source level of 10 Pa, it measured –37.6 dBV. Therefore the sensitivity of the calibrator microphone is about –2.7e-7 Volt/SPL.

Use the HP analyzer to apply a source voltage of 1V at 178 Hz to the side-mounted speaker. Remove one tap of the pressure transducers at the middle of the tube, and insert the high sensitivity microphone to the same location. The pressure sensed is about 107.6dB SPL, or 4.7997 Pa. Mount the pressure transducer back to the same tap, and measure the voltage from the pressure transducer. The gain setting on an amplifier was 200 as it was set for all experimental measurement. The sense the voltage by the transducer was 0.156 Vrms, or 0.221 Volt. So, the sensitivity of pressure transducer is 0.046 Volt/Pa, or 0.0326 Vrms/Pa. It also is equivalent to 9.2e-7 V/SPL.

Appendix C. Details of the Acoustic Model Development

The acoustic wave equation with heat release as forcing is showed in (6.6),

$$\frac{\partial^2 p'}{\partial t^2} - \bar{c}^2 \frac{\partial^2 p'}{\partial x^2} = (\gamma - 1)\frac{dq'(t)}{dt}\delta(x - x_f)$$

where sound speed $\bar{c} = \sqrt{\gamma \frac{\bar{p}}{\rho_0}}$. The equation can also be written as,

$$\rho_0 \frac{\partial^2 p'}{\partial t^2} - \gamma p_0 \frac{\partial^2 p'}{\partial x^2} = \rho_0(\gamma - 1)\frac{dq'(t)}{dt}\delta(x - x_f) \qquad \text{(C.1)}$$

The Rijke tube with length L is closed at $x = 0$, and open at the other end $x = L$. The boundary conditions are,

$$\left.\frac{\partial p}{\partial x}\right|_{x=0} = 0, \;\; p(L) = 0 .$$

The oscillatory pressure can be expanded in orthogonal acoustic modes as in (6.7)

$$p'(x,t) = \sum_{i=1}^{\infty} \psi_i(x)\eta_i(t)$$

Using the boundary conditions, we can compute the wave number $k_i = \frac{2i-1}{2L}\pi$ and mode function $\psi_i(x) = A_i \cos(k_i x)$. Normalize the modes using orthogonality,

$$\int_0^L \rho_0 \psi_i \psi_j dx = \delta_{ij} \qquad \text{(C.2)}$$

It is also equivalent to,

$$\int_0^L \gamma \bar{p} \psi_i \frac{d^2 \psi_j}{dx^2} dx = -\omega_{i(j)}^2 \delta_{ij} \tag{C.3}$$

Substituting the modal function to the above equation, we can obtain the amplitude of the mode A_i,

$$A_i = \sqrt{\frac{2}{\rho_0 L}}, \text{ and } \psi_i(x) = \sqrt{\frac{2}{\rho_0 L}} \cos(\frac{2i-1}{2L}\pi x).$$

Notice that

$$\int_0^x \psi_i(x) = -\frac{1}{k_i^2} \psi_i'(x)$$

Plug the mode function into the (C.1),

$$\sum_{i=1}^{\infty} \rho_0 \ddot{\eta}_i \psi_i - \sum_{i=1}^{\infty} \eta_i \gamma \bar{p} \frac{d^2 \psi_i}{dx^2} = \rho_0 (\gamma - 1) \frac{dq'(t)}{dt} \delta(x - x_f) \tag{C.4}$$

Multiply through by mode shape and integrate over the domain by orthogonality,

$$\ddot{\eta}_i + \omega_i \eta_i = \rho_0 (\gamma - 1) \left[\int_0^L \psi_i(x) \delta(x - \frac{L}{2}) \right] \frac{dq'(t)}{dt},$$

and for each mode, it becomes,

$$\ddot{\eta}_i + \omega_i \eta_i = \rho_0 (\gamma - 1) \sqrt{\frac{2}{\rho_0 L}} \cos(\frac{2i-1}{4}\pi) \frac{dq'(t)}{dt} \tag{C.5}$$

The output velocity fluctuation *u*' can be computed from (6.5). For upstream locations $x < x_f$, it becomes,

$$\frac{\partial p'}{\partial t} + \gamma \bar{p} \frac{\partial u'}{\partial x} = 0 \tag{C.6}$$

Integrating over the spatial domain, it results

$$u'(x,t) - u'(0,t) = -\sum_{i=1}^{\infty} \frac{1}{\gamma \bar{p}} \dot{\eta}_i(t) \int_0^x \psi_i(x) dx \tag{C.7}$$

The boundary condition gives that $u'(0,t) = 0$ at the closed end. Therefore, the velocity perturbation *u*' just below the flame holder is

$$u'(x,t)\big|_{x=x_f} = -\sum_{i=1}^{\infty} \frac{1}{\gamma \bar{p}} \dot{\eta}_i(t) \int_0^{x_f} \psi_i(x) dx \tag{C.8}$$

At the flame location $x = x_f$, the velocity fluctuation is,

$$u'_f(t)\Big| = -\sum_{i=1}^{\infty} \frac{1}{\gamma \bar{p} k_i} \sqrt{\frac{2}{\rho_0 L}} \sin\left(\frac{2i-1}{4}\pi\right) \dot{\eta}_i(t) \tag{C.9}$$

Equations (C.5)(C.9) developed above give the theoretical acoustic model for the Rijke tube. With the assumption of cold flow at inlet temperature, the first mode frequency is 60 Hz, and the second mode frequency is 180 Hz.

As we saw earlier from Figure 6.4 about the measured cold tube acoustic resonance frequencies, the first mode is at about 56 Hz, and the second mode is near 163 Hz. Considering the radiation impedance at the open end of the Rijke tube, it will equivalently extend the length of the combustor. As a result, the modal frequency will be smaller than 60 and 180 Hz.

Meanwhile, considering the effects of the mean heat in the combustor, the temperature effect should be considered. As the temperature *T* increases, sound speed *c* is also increased, which is proportional to $\sqrt{T}$. As a result, this will effectively shorten the length of the tube, and modal frequency will be higher than the cold measurements. In our two-mode linear acoustic model, those effects are not considered for simplicity, but the acoustic modal frequencies qualitatively matches the actual combustor acoustic resonance.

Appendix D. Linear Flame Data Measured by Experiments

Equivalence Ratio ϕ	Flow rate Q_{tot} (cc/s)	Frequency (Hz)	Gain (dB)	Phase (deg)
0.55	100	175	-26.1097	-66.8278
		180	-26.8781	-80.2529
		185	-26.4213	-62.8270
0.55	110	175	-20.3632	-68.5951
		180	-21.14912	-71.0420
		185	-22.9432	-62.5439
0.55	120	175	-15.8248	-54.2589
		180	-16.1099	-61.3210
		185	-18.4732	-56.6570
0.55	130	175	-10.6979	-60.9310
		180	-11.7679	-54.5480
		185	-12.8688	-62.3759
0.55	140	175	-6.9324	-37.9632
		180	-7.5770	-39.4170
		185	-8.5825	-40.8213
0.55	160	175	-1.9683	-26.4657
		180	-3.2352	-29.5600
		185	-3.6266	-31.5764
0.55	180	175	2.7713	-12.9280
		180	2.2351	-14.3455
		185	1.0463	-18.3677

Table D.1 Linear flame data for ϕ = 0.55 with different flow rates

Equivalence Ratio ϕ	Flow rate Q_{tot} (cc/s)	Frequency (Hz)	Gain (dB)	Phase (deg)
0.55	180	180	2.2351	-14.3455
0.60	160	180	2.9818	12.5010
0.60	180	180	8.0311	33.6014
0.65	160	180	9.4765	46.5492
0.65	180	180	14.4673	61.4693

Table D.2 Linear flame data for large equivalence ratios (quartz chimney)

Equivalence Ratio ϕ	Flow rate Q_{tot} (cc/s)	Frequency (Hz)	Gain (dB)	Phase (deg)
0.55	180	180	1.5799	-16.2980
0.60	160	180	1.9311	-4.2300
0.60	180	180	5.7465	12.2810
0.65	160	180	7.1257	16.5410
0.65	180	180	12.5258	29.4090

Table D.3 Linear flame data for large equivalence ratios (steel chimney)

Since the instrumental setup is about the same, the linear flame data listed above is in line with the experimental data captured by Khanna et al. [Kha01] The only difference is that we manually add an 180^{o} phase correction based on our observation of the negative sign of the OH* signal. Table D.4 lists the steady-state measurement data as an example. As equivalence ratio increases, the OH* should increase accordingly.

Equivalence Ratio ϕ	Flow rate Q_{tot} (cc/s)	OH* voltage level (volt)
0.5260	173.389	-0.67 ~ -0.69
0.6146	174.668	-0.85 ~ -0.875
0.7239	176.755	-1.06 ~ -1.08
0.8333	178.653	-1.39 ~ -1.42

Table D.4 Steady state OH* measurement

Appendix E. Nonlinear Flame Experimental Data

Frequency (Hz)	Input Amplitude (V)	Output Amplitude (V)	Output Gain	Output Phase (deg)	Speaker Voltage (V)
175	0.059	0.0151	0.24897	-48.8107	0.2
180	0.053	0.0127	0.22762	-51.8563	0.2
185	0.049	0.0104	0.19782	-55.0087	0.2
175	0.146	0.0349	0.23672	-51.0496	0.5
180	0.135	0.0299	0.21941	-51.9926	0.5
185	0.125	0.0269	0.21343	-53.3733	0.5
175	0.302	0.0682	0.2254	-50.4145	1
180	0.279	0.0622	0.22284	-51.1031	1
185	0.257	0.0507	0.19662	-51.7684	1
175	0.460	0.0978	0.21221	-51.6562	1.5
180	0.422	0.0853	0.20205	-52.1839	1.5
185	0.393	0.0744	0.18871	-53.5701	1.5
175	0.606	0.1093	0.18019	-52.8256	2
180	0.557	0.0966	0.17335	-53.2463	2
185	0.523	0.0951	0.18142	-54.2427	2
175	0.84	0.1451	0.17263	-57.4228	3
180	0.784	0.1303	0.16601	-57.8049	3
185	0.741	0.1174	0.15822	-58.3755	3
175	1.040	0.1539	0.14778	-59.1918	4
180	0.959	0.1424	0.14836	-60.7370	4
185	0.909	0.1329	0.14612	-61.4924	4
175	1.219	0.1566	0.12821	-65.8533	6
180	1.155	0.1559	0.13484	-64.7257	6
185	1.102	0.1433	0.12991	-64.2926	6

Table E.1 Experimental flame describing function for $\phi = 0.55$, $Q_{tot} = 130$ cc/s

Frequency (Hz)	Input Amplitude (V)	Output Amplitude (V)	Output Gain	Output Phase (deg)	Speaker Voltage (V)
175	0.069	0.0530	0.76584	-27.8556	0.2
180	0.063	0.0445	0.70272	-28.2028	0.2
185	0.059	0.0391	0.66194	-30.2012	0.2
175	0.172	0.1250	0.72586	-27.6610	0.5
180	0.158	0.1109	0.69971	-29.1751	0.5
185	0.147	0.0932	0.63275	-31.6270	0.5
175	0.347	0.2138	0.61596	-28.5014	1
180	0.319	0.1916	0.60059	-29.7146	1
185	0.295	0.1687	0.57149	-31.5919	1
175	0.503	0.2216	0.43987	-24.8674	1.5
180	0.473	0.2181	0.46088	-29.8097	1.5
185	0.444	0.2027	0.45621	-32.8617	1.5
175	0.595	0.2197	0.36917	-2.32870	2
180	0.568	0.2103	0.37025	-11.3498	2
185	0.550	0.2091	0.37960	-20.3759	2
175	0.846	0.3094	0.36554	-358.736	3
180	0.782	0.2819	0.36028	-1.04040	3
185	0.743	0.2614	0.35168	-5.02250	3
175	1.124	0.3581	0.31840	-10.4643	4
180	1.021	0.3421	0.33496	-7.71660	4
185	0.938	0.3141	0.33464	-10.8480	4
175	1.323	0.3692	0.27886	-20.5862	6
180	1.212	0.3639	0.29995	-15.5026	6
185	1.102	0.3449	0.31253	-12.2715	6
175	1.182	0.3692	0.31197	-32.5602	8
180	1.201	0.3391	0.28196	-30.8644	8
185	1.143	0.3464	0.30228	-18.9827	8

Table E.2 Experimental flame describing function for $\phi = 0.55$, $Q_{tot} = 160$ cc/s

Frequency (Hz)	Input Amplitude (V)	Output Amplitude (V)	Output Gain	Output Phase (deg)	Speaker Voltage (V)
175	0.058	0.0931	1.59454	-353.328	0.2
180	0.056	0.0871	1.55049	-354.515	0.2
185	0.055	0.0795	1.44713	-358.359	0.2
175	0.148	0.2193	1.47661	-355.181	0.5
180	0.14	0.1981	1.41358	-356.898	0.5
185	0.136	0.1832	1.34777	-1.0976	0.5
175	0.307	0.3613	1.17766	-1.4218	1
180	0.282	0.3325	1.17884	-3.3343	1
185	0.267	0.3109	1.16616	-4.6256	1
175	0.475	0.4455	0.93711	-9.3913	1.5
180	0.432	0.4241	0.98107	-8.3504	1.5
185	0.402	0.4079	1.01466	-10.1184	1.5
175	0.638	0.5141	0.80582	-16.5343	2
180	0.579	0.5053	0.87245	-15.3332	2
185	0.531	0.4769	0.89757	-16.1477	2
175	0.835	0.5407	0.64716	-17.6141	3
180	0.83	0.5703	0.68633	-18.9768	3
185	0.738	0.5585	0.75587	-17.7921	3
175	0.901	0.5777	0.64104	-334.674	4
180	0.89	0.5199	0.58352	-350.356	4
185	0.897	0.5163	0.57524	-4.2541	4
175	1.155	0.6838	0.59099	-349.475	6
180	1.031	0.6519	0.63207	-338.738	6
185	0.873	0.6037	0.69061	-337.425	6
175	1.378	0.7201	0.52145	-15.5838	8
180	1.321	0.708	0.53505	-356.222	8
185	1.263	0.735	0.58064	-338.552	8

Table E.3 Experimental flame describing function for $\phi = 0.6$, $Q_{tot} = 160$ cc/s

Frequency (Hz)	Input Amplitude (V)	Output Amplitude (V)	Output Gain	Output Phase (deg)	Speaker Voltage (V)
175	0.076	0.1004	1.32258	-13.1345	0.2
180	0.07	0.0869	1.23024	-14.9899	0.2
185	0.066	0.0759	1.14587	-17.1489	0.2
175	0.184	0.2168	1.17973	-13.2447	0.5
180	0.172	0.1985	1.15485	-15.1914	0.5
185	0.162	0.1705	1.05295	-17.5111	0.5
175	0.368	0.3551	0.96565	-15.7962	1
180	0.338	0.3342	0.98809	-17.3966	1
185	0.317	0.3004	0.94694	-19.1507	1
175	0.529	0.4146	0.78286	-20.2168	1.5
180	0.488	0.3943	0.80775	-20.9192	1.5
185	0.452	0.3723	0.82259	-23.0039	1.5
175	0.672	0.4157	0.61861	-13.4331	2
180	0.637	0.4194	0.65775	-17.9956	2
185	0.606	0.4272	0.70502	-23.3721	2
175	0.755	0.3709	0.49111	-327.601	3
180	0.726	0.3244	0.44647	-333.727	3
185	0.697	0.2931	0.42017	-344.002	3
175	1.083	0.549	0.50656	-346.825	4
180	0.974	0.5117	0.52533	-341.206	4
185	0.887	0.4687	0.52851	-340.066	4
175	1.386	0.5522	0.39828	-8.5882	6
180	1.258	0.5525	0.43894	-1.0284	6
185	1.157	0.5365	0.46356	-358.018	6
175	1.327	0.554	0.417	-23.9392	8
180	1.324	0.5613	0.42374	-15.4413	8
185	1.25	0.5563	0.44444	-5.7972	8
175	1.084	0.5322	0.49016	-34.6378	10
180	1.173	0.5431	0.4625	-24.3519	10
185	1.174	0.5515	0.46929	-15.3851	10

Table E.4 Experimental flame describing function for $\phi = 0.55$, $Q_{tot} = 180$ cc/s

Frequency (Hz)	Input Amplitude (V)	Output Amplitude (V)	Output Gain	Output Phase (deg)	Speaker Voltage (V)
175	0.048	0.1194	2.47679	-323.292	0.2
180	0.047	0.1104	2.3509	-326.7	0.2
185	0.046	0.1036	2.23582	-329.453	0.2
175	0.13	0.2909	2.23554	-328.713	0.5
180	0.124	0.2671	2.15718	-330.421	0.5
185	0.12	0.2519	2.10467	-333.043	0.5
175	0.289	0.5581	1.92953	-343.484	1
180	0.264	0.5164	1.95373	-343.9	1
185	0.251	0.4868	1.94138	-346.18	1
175	0.627	0.8597	1.37007	-2.731	2
180	0.559	0.8193	1.46444	-0.271	2
185	0.514	0.7733	1.50517	-1.0822	2
175	1	0.8441	0.84267	-339.84	4
180	1.072	0.8406	0.78356	-359.952	4
185	1.024	0.8546	0.83433	-7.5194	4
175	0.689	1.0688	1.53634	-325.111	6
180	0.523	0.9789	1.83509	-311.119	6
185	0.439	0.8547	1.90779	-328.77	6
175	1.569	1.0456	0.6646	-16.2361	8
180	1.162	1.0506	0.89433	-342.899	8
185	0.93	1.0343	1.0983	-318.895	8

Table E.5 Experimental flame describing function for $\phi = 0.6$, $Q_{tot} = 180$ cc/s

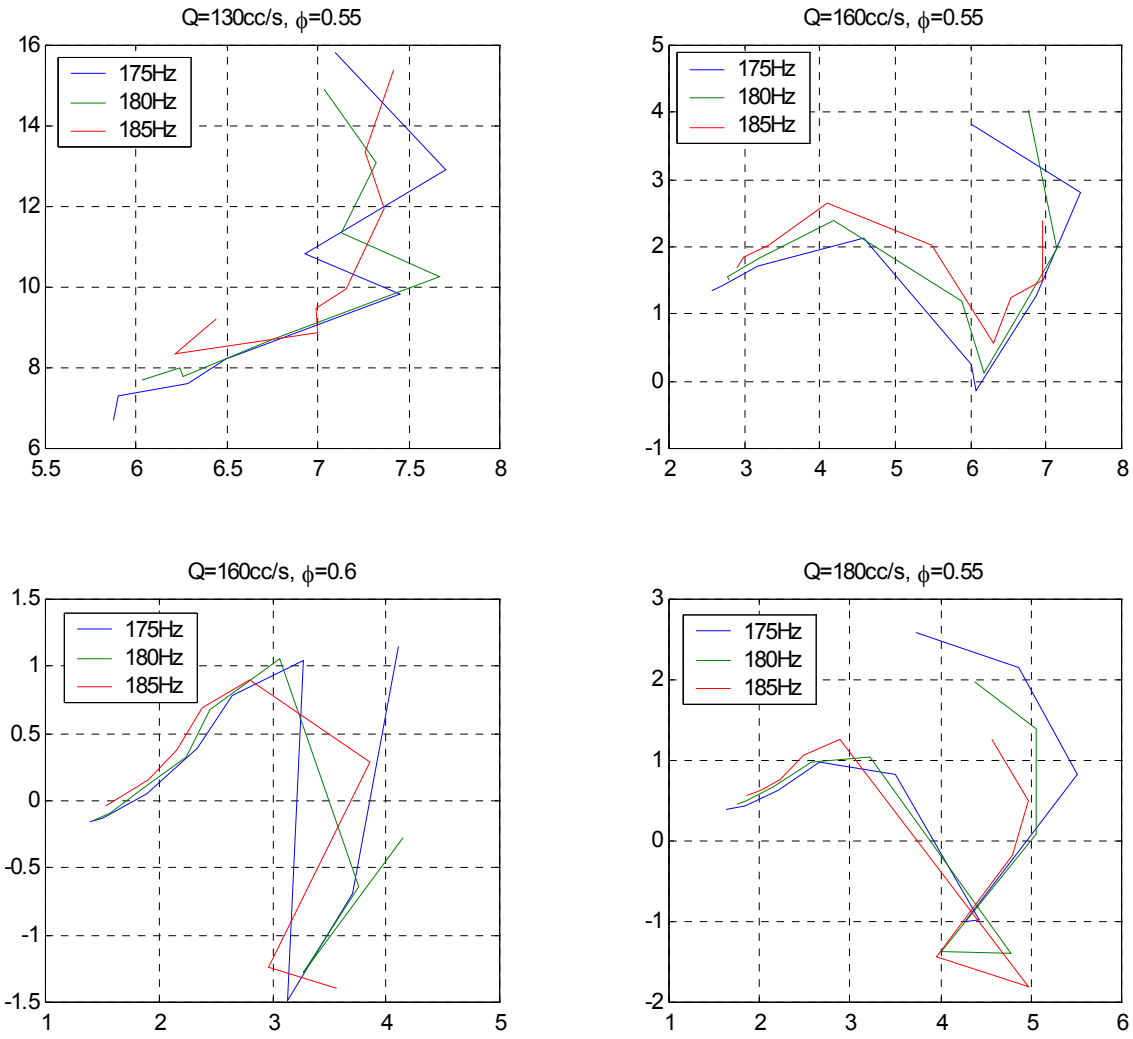

Figure E.1 Plots of 1/N(A,ω) on the Nyquist diagram

Vita

Xinming Huang was born in Jiangsu, China on Oct. 1974. He graduated from Nantong High School in 1991, and was selected to enroll in the teaching-innovation program of Northwestern Polytechnic University in Xi'an, China. In 1994, he completed the four-year undergraduate program with one year in advance, and received B. Sc. in Mechanical Engineering. Upon completion of his master's degree in Electrical Engineering there in 1996, he was working and studying on a joint-cultivated program in Penang, Malaysia. Later in 1997, he joined GenRad Inc. as an applications engineer in Science Park, Singapore. Since fall 1998, he has been a research assistant with Dr. Baumann, working towards his Ph.D. degree in Electrical Engineering in Virginia Tech. His research focused on reduced-order modeling and system identification techniques for complicated nonlinear system, including partial differential equation, model order reduction, experimental describing function and limit cycle analysis. Current research interests also include adaptive filter, digital signal processing algorithms, and nonlinear model identification. Upon completion his degree, he is currently working as a member of technical staff in the advanced wireless technology labs of Lucent Technologies.